Tectonophysics, 175 (1990) 249–268
Elsevier Science Publishers B.V., Amsterdam – Printed in The Netherlands

Temporal variations in seismicity during quasi-static and dynamic rock failure

PHILIP G. MEREDITH [1], IAN G. MAIN [2*] and COLIN JONES [1]

[1] *Department of Geological Sciences, University College London, Gower Street, London WC1E 6BT (U.K.)*
[2] *Department of Geosciences, University of Reading, Whiteknights, Reading RG6 2AB (U.K.)*
* *Presently at: Department of Geology and Geophysics, University of Edinburgh, Mayfield Road, Edinburgh EH9 3JZ (U.K.)*

(Received by publisher May 9, 1989)

Abstract

Meredith, P.G., Main, I.G. and Jones, C., 1990. Temporal variations in seismicity during rock failure. In: S. Das and M. Ohnaka (Editors), Earthquake Source Processes. *Tectonophysics*, 175: 249–268.

A comprehensive model is presented which can explain temporal fluctuations in seismic *b*-values in the period leading to mechanical failure in terms of the underlying physical processes of time-varying applied stress and stress corrosion-enhanced crack growth under conditions of constant strain rate. The form of the *b*-value anomaly in the period leading to failure depends on the form of the stress/time relationship. For the case where dynamic failure occurs at peak stress after a period of strain hardening, the model predicts a single cusp-like *b*-value anomaly, reaching a critically low value of 0.5 at failure. For the physically most realistic case where dynamic failure is preceded by a period of precursory strain energy release during strain softening, the model predicts two minima in the *b*-value, separated by a temporary maximum or inflection point. These fluctuations in the *b*-value are consistent with reported "intermediate-term" and "short-term" earthquake precursors separated by a period of seismic quiescence. For the case of quasi-static cataclastic flow, the *b*-value mirrors the stress and never falls to the critical value because there is no critical rupture.

New results from a series of controlled laboratory experiments are presented in which microseismic event rates and *b*-values were monitored contemporaneously with stress/time data for all variants of the stress/time relationship. Recent field observations of temporal changes in seismicity rates and *b*-value preceding major earthquakes are also reported. Both data sets exhibit *b*-value anomalies which are consistent with the model predictions.

Introduction

Rock failure by localised fault generation is rarely, if ever, the result of a linearly time-increasing applied stress leading to dynamic rupture at some peak failure stress. If it were, it would be a relatively simple matter to predict the time of failure from knowledge of the initial stress conditions and the rate of stress input (Shimazaki and Nakata, 1980; Main, 1988). In heterogeneous natural materials, dynamic rupture is nearly always preceded by a period of inelastic strain hardening, and commonly also by a period of strain softening following the peak stress (e.g. Paterson, 1978; Stuart, 1979a). These inelastic phases are due to the time-dependent growth and coalescence of microcracks or small faults preceding macroscopic failure, or precursory slip on an established fault. A considerable body of experimental and theoretical evidence suggests that much of this time-dependent brittle behaviour of rocks is due to the subcritical growth of small cracks by the mecha-

0040-1951/90/$03.50

nism of stress corrosion in the presence of chemically active environmental species such as water (e.g. Anderson and Grew, 1977; Atkinson, 1982; Atkinson and Meredith, 1987a; Costin, 1987). Indeed, Das and Scholz (1981) have been able to use a simple fracture mechanics model, based on stress corrosion-enhanced growth of a penny-shaped shear crack in response to a constant applied stress, in order to explain qualitatively all of the observed forms of time-dependent phenomena associated with earthquake rupture.

It is this inelastic phase of the loading cycle, and its associated crack growth and release of strain energy, which gives rise to a range of seismic precursors to failure. In the earth, precursors that have been cited as being of statistical significance include (1) spatial and temporal variations in wave propagation parameters such as seismic velocity ratios and scattering attenuation (e.g. Rikitake, 1976; 1987; Jin and Aki, 1986), and (2) variations in seismicity statistics such as event rates (e.g. Wyss et al., 1984; Wyss, 1986) and seismic *b*-values (e.g. Jin and Aki, 1986; Smith, 1981; 1986). Changes in seismicity statistics have the potential to be the more sensitive predictors of the approach to failure because they sample the contemporary growth and coalescence of fractures, whereas wave propagation parameters respond to the cumulative influence of fractures. In the laboratory, acoustic emission (microseismic) event rates have already been shown to be directly related to the growth rate of cracks in rocks (e.g. Sano and Ogino, 1980; Atkinson and Rawlings, 1981; Meredith and Atkinson, 1983), and acoustic emission *b*-values have been linked to rock heterogeneity (Mogi, 1967), the level of applied stress (Scholz, 1968a) and changes in fracture mechanism (Meredith and Atkinson, 1983).

In this paper we present a comprehensive model to explain temporal variations in seismic *b*-values for a variety of forms of time-varying applied stress under conditions of a constant remote strain rate and crack growth dominated by environmentally enhanced stress corrosion. The model predictions are compared with direct observations of *b*-value variations from both laboratory-scale rock fracture experiments and recent major earthquakes.

Theory

Fracture mechanics

In this section we apply the fracture mechanics approach of Lawn and Wilshaw (1975) to rock failure under a variety of conditions in order to model, where appropriate, variations in stress intensity over the complete cycle of loading, quasi-static failure and dynamic failure. Although a number of estimates of the fracture energy for dynamic shear failure have been reported for both laboratory-sized samples and crustal faults (tabulated in Li, 1987), it is unlikely that stress intensities for shear fracture will be directly measured in the earth in the near future, especially for the case of subcritical fracture. However, we present here a theory which shows that it may be possible to monitor remotely changes in the stress intensity by inference from observations of variations in the seismic *b*-value. Some aspects of this model have already been presented elsewhere (Main, 1988; Main et al., 1989; Main and Meredith, 1989). but a comprehensive description is presented here for reference purposes.

As Stuart (1979a) has pointed out, the frequently-stated assertion that earthquakes occur when the peak stress is reached may be incorrect for the real earth. Many laboratory examples show that elastic loading may be followed by a phase of strain hardening due to microcracking and dilatancy, and then a strain softening phase following the peak stress (Paterson, 1978; Lama and Vutukuri, 1978). We define "quasi-static failure" as occurring when the peak stress is reached, because a fault develops at this stage and begins to rupture at a subcritical velocity, and we define "dynamic failure" as occurring when a crack extends or a fault ruptures at a velocity approaching the sonic velocity of the medium. It is an empirical fact that dynamic failure in laboratory experiments usually occurs at a period of decreasing stress. A number of mechanisms have been proposed to explain this precursory decrease in stress: crack coalescence following dilatancy (Miachkin et al., 1972), an increase in pore fluid pressure following dilatancy (Scholz et al., 1973), or precursory slip behind a growing crack front

(Stuart, 1979b). All of these mechanisms are likely to occur in the earth, with crack coalescence being dominant in the early phase of precursory stress decrease and precursory slip dominating the final nucleation phase before catastrophic crack extension (Main and Meredith, 1989).

Because earth materials contain flaws on all scales (dislocations, microcracks, joints, faults, etc.), it is evident that the distribution of such flaws will influence their physical and mechanical properties, and changes in the flaw distribution will induce corresponding changes in these properties. Following the fracture mechanics approach of Lawn and Wilshaw (1975), we assume that prior to catastrophic rupture there exists one major fault and a number of minor faults which contribute only negligibly to the fracture energy. This appears to be a realistic assumption because, for example, aftershocks commonly radiate only a few percent of the seismic energy of a mainshock (Båth, 1981). We assume further that a segment of the fault is free to move and that dynamic rupture is restrained by an asperity or strong patch ahead of the crack tip. If the length of the free segment is X, and the remotely applied stress is σ_r the resulting stress concentration at the crack tip, for any mode of crack tip displacement, can be expressed in terms of the stress intensity factor (K) where:

$$K = Y\sigma\sqrt{X} \tag{1a}$$

and

$$\sigma = \sigma_r - \sigma_{fr} - \sigma_p \tag{1b}$$

Y is a geometrical factor which is tabulated for a wide range of crack configurations (e.g. Sih, 1973; Rooke and Cartwright, 1976), σ is the effective remote stress, σ_{fr} is the frictional stress on the free segment, and σ_p is the pore fluid pressure.

The crack may extend dynamically at a critical rate close to the sonic velocity of the medium, or quasi-statistically at subcritical velocities by one or more of a number of competing mechanisms (Atkinson, 1982; 1984; Atkinson and Meredith, 1987a). These include stress corrosion, dissolution, diffusion, ion exchance and microplasticity, all of which are influenced by the chemical effects of pore fluids in the crustal environment. However, it should be noted that subcritical crack growth is possible even in the absence of chemical agents. Close to the critical stress intensity for dynamic rupture there exists a range of stress intensities and crack tip positions in which the crack is stable due to the discrete nature of the crystalline lattice. The crack is said to be "lattice-trapped", and a sufficient input of thermal energy can allow the crack to extend from one position of stability to another (Lawn, 1975; Atkinson and Meredith, 1987a). The role of any extrinsic, chemically enhanced mechanism may therefore be viewed as an enhanced activation of the intrinsic bond rupture process. Recent reviews of quasi-static crack growth in geological materials (Anderson and Grew, 1977; Atkinson, 1982; 1984; Atkinson and Meredith, 1987a) have all concluded that the overwhelming body of evidence suggests that stress corrosion is likely to be the dominant mechanism of subcritical crack growth in the seismogenic zone of the crust. The strongest reagent for the stress corrosion process is water, but the crack extension velocity also depends on temperature, pressure and rock composition.

A number of constitutive equations have been proposed to decribe the relationship between stress intensity factor and crack extension velocity ($\dot{X}$) during stress corrosion-controlled subcritical crack growth (reviewed by Anderson and Grew (1977) and Atkinson (1982)). The most commonly used equations to date have been the Charles (1958) power law relationship and the Wiederhorn and Bolz (1970) modification of the Charles and Hillig (1962) exponential relationship, both of which are based on reaction rate theory. The Charles (1958) equation is much more readily integrated for prediction of the time-dependent failure properties of rocks (e.g. Atkinson, 1980; Lankford, 1981; Sano et al., 1982). In this paper we follow the vast majority of experimental studies on geological materials (see Atkinson and Meredith, 1987a) and modelling studies of geological problems (e.g. Demarest, 1976; Das and Scholz, 1981) in using the Charles power to describe the $\dot{X}$–K relationship during stress corrosion-enhanced subcritical crack growth. In its simplest form this may be written as:

$$\dot{X} = V_0(K/K_0)^n \tag{2}$$

where V_0 and K_0 are initial values of the crack velocity and stress intensity factor at time t_0, and n is the stress corrosion index. Empirically, for tensile crack growth at least, the value of n is generally found to be in the range 20–60 for earth materials (Atkinson and Meredith, 1987b); the acceleration to dynamic fracture is therefore a highly non-linear but not instantaneous process. There is as yet no direct evidence that eqn. (2) holds for shear fracture propagation, but there appears to be no good physical reason to suppose that the form of the relationship will vary with crack mode (Das and Scholz, 1981), although the values of the constants (V_0, K_0 and n) may change. If the initial stress intensity factor is $K_0 = Y\sigma_0\sqrt{X_0}$, then:

$$\dot{X} = V_0\left\{\left[\sigma(t)\cdot\sqrt{X}(t)\right]/\left[\sigma_0\cdot\sqrt{X_0}\right]\right\}^n \quad (3)$$

A complete solution of this differential equation would require a numerical approach, including a constitutive relationship between the amount of precursory slip, the crack extension velocity and the stress. However, the equation can be solved analytically to a first order by truncating a Taylor expansion of a time-dependent applied stress σ with $t_0 = 0$:

$$\sigma(t) = \sigma_0 + a_1 t + a_2 t^2 + \ldots a_i t^i + \ldots \quad (4)$$

If, for example, a load is applied at some remote boundary at a constant rate of strain, such as by the relative motion of two lithospheric plates moving at their terminal velocities, an elastic build-up of strain energy implies that $a_1 = \dot{\sigma}$, the rate of stress increase, and $a_i = 0$ for $i \geq 2$. If σ_0 is the residual stress averaged over the free-slipping and asperity segments subsequent to an event, the potential stress drop $\Delta\sigma$ is $(\sigma - \sigma_0)$ for a slip-predictable model (Shimazaki and Nakata, 1980). In the earth, the potential stress drop averaged over the whole fault (30–100 bars, Kanamori, 1978) is much smaller than the effective shear resistance at earthquake nucleation depths (order of 1 kbar, Sibson, 1982). Therefore, the first-order term (σ_0 = constant) in eqn. (4) dominates the expansion. Note that $\sigma_0 > \sigma_{fr}$, because the stress drop on asperities is much higher than that on the free-slipping segment. Thus the model presented here is, in principle, capable of including frictional effects via σ_{fr}, whereas earlier models (Das and Scholz, 1981; Main, 1988) assumed $\sigma_{fr} = 0$. The effect of the second-order time-dependent term a_2 is similarly much less than that of the first-order time-dependent term a_1 for the real earth, because non-linearity may only occur in the last ~ 5% of the earthquake cycle (Stuart, 1988). This implies that to a good approximation we can truncate the expansion at two terms, and hence treat eqn. (3) as a separable equation. The solution (Das and Scholz, 1981; Main, 1988) is:

$$X = X_0\left\{1 - [(n-2)/2](V_0 t/X_0) \times \left[1 + (n\dot{\sigma}t/2\sigma_0)\right]\right\}^{2/(2-n)} \quad (5)$$

where the dynamic failure time (t_f), defined by $X/X_0 \to \infty$, is:

$$t_f = [2/(n-2)](X_0/V_0)/[1 + (n\Delta\sigma/2\sigma_0)] \quad (6)$$

Note that even for the case of constant stress (i.e. $\dot{\sigma} = 0$) the crack will accelerate by stress corrosion to critical rupture. The form of eqn. (5) can be further simplified to a good approximation to:

$$X = X_0(1 - t/t_f)^{2/(2-n)} \quad (7)$$

For a typical range of $20 < n < 60$, this implies a highly non-linear acceleration from quasi-static subcritical crack growth to critical dynamic rupture.

Stress intensity and the seismic b-value

The seismic b-value is currently the only remotely sensed parameter which has been experimentally correlated with stress intensity (Meredith and Atkinson, 1983). The relevant data, obtained by monitoring acoustic emission activity during laboratory-scale fracture experiments, are given in Fig. 1, which also includes more recent results (S. Clifford, unpublished data, 1988). We make qualitative use of these results even though they were determined for tensile crack growth because, as we have noted earlier, there is no physical reason why the stress corrosion process should depend on mode of fracture, and because no such results are available for shear modes. The data clearly illustrate that b is negatively correlated

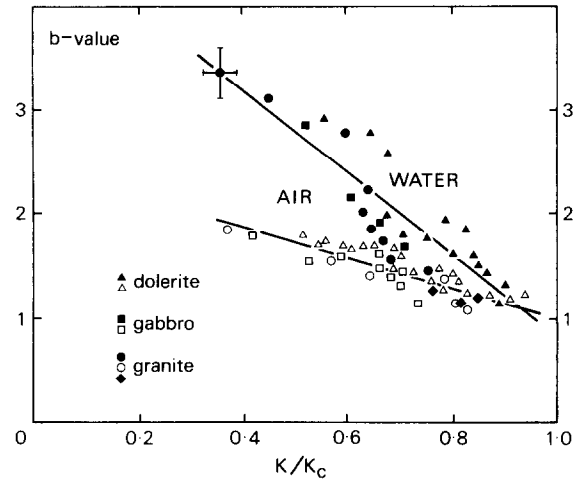

Fig. 1. Synoptic diagram of the variation in b-value with stress intensity and crack tip "humidity" for a variety of crystalline rocks. The data were derived from tensile crack growth experiments performed at ambient pressure and temperature using the double torsion technique. Stress intensity factors have been normalised with respect to the critical stress intensity factor for catastrophic failure, or fracture toughness. For all the rock types tested, fracture in a nominally dry environment (air) produced systematically lower b-values than in water, and high stress intensity factors are correlated with low b-values. Lines show least-squares fits to the data points and converge at approximately the point ($K/K_c = 1$, $b_c = 1$), irrespective of rock type. Data are taken from Meredith and Atkinson (1983) and S. Clifford (unpublished data, 1988).

and linearly related to K via an expression of the form:

$$b = p - qK \tag{8}$$

where p and q are positive constants, and:

$$\log N = a - bm \tag{9}$$

is the discrete frequency–magnitude relationship of either earthquakes or acoustic emissions. N is the number of times a magnitude in the range $(m - \delta m/2) < m < (m + \delta m/2)$ occurs where δm is the magnitude discrimination interval, and a and b are empirical constants. For the experimentally derived data of Meredith and Atkinson (1983), b-values are found to lie in the range 1–3, with dynamic rupture occurring when $b = 1$ and the stress intensity factor reaches its critical value, K_c (Fig. 1). For "wet" samples both p and q are greater than for nominally "dry" samples. Changes in the b-value may therefore be due either to changes in stress intensity or to changes in the chemical activity of corrosive environmental species. In the earth, $0.5 < b < 1.5$ and the critical b-value, evaluated from foreshock sequences, is 0.5 (Von Seggern, 1980). The difference between the laboratory data (shown in Fig. 1) and the field observation can be explained by considering a power law distribution of crack or fault lengths of exponent D, in some range X_{min}–X_{max}, so that:

$$N(X) = CX^{-D} \tag{10}$$

where C is a constant. If the seismic moment (M_0) may be related to the magnitude (m) by:

$$M_0 = 10^{cm+d} \tag{11}$$

where c and d are constants (Kanamori, 1978), several authors (e.g. Caputo, 1976; Aki, 1981; King, 1983) have shown that:

$$D = 3b/c \tag{12}$$

Furthermore, if the distributed faults are geometrically scale invariant between X_{min} and X_{max}, D would be strictly defined as one of the fractal dimensions of the system (Mandelbrot, 1982; Turcotte, 1989). For the experimental results of Fig. 1, the relative time constants of the events and the recording instrument imply, from a simple dislocation model (Kanamori and Anderson, 1975; Main et al., 1989), that $c = 3$, so that $b = D$. For intermediate-sized earthquakes, $c = 3/2$ (Kanamori, 1978) and therefore $b = 2D$. From eqn. (10) it can be shown that the average crack length becomes unstable when $D = 1$ (Main, 1988), corresponding to critical crack coalescence. Thus we can reconcile the laboratory and field results by limiting D to the range 1–3, with a critical value of $D_c = 1$ at catastrophic failure. The upper bound is determined by the Euclidean dimension (a volume) within which the faults are contained.

Thus stress intensity can be related directly to the seismic b-value via p and q, and by inference from the length distribution of faults or microcracks (D) via eqn. (12). It is important to note that it is D which is the more fundamental parameter, and that b is also a function of the event duration and the recording system.

Model predictions

In this section the model predictions for the behaviour of the b-value anomaly are determined

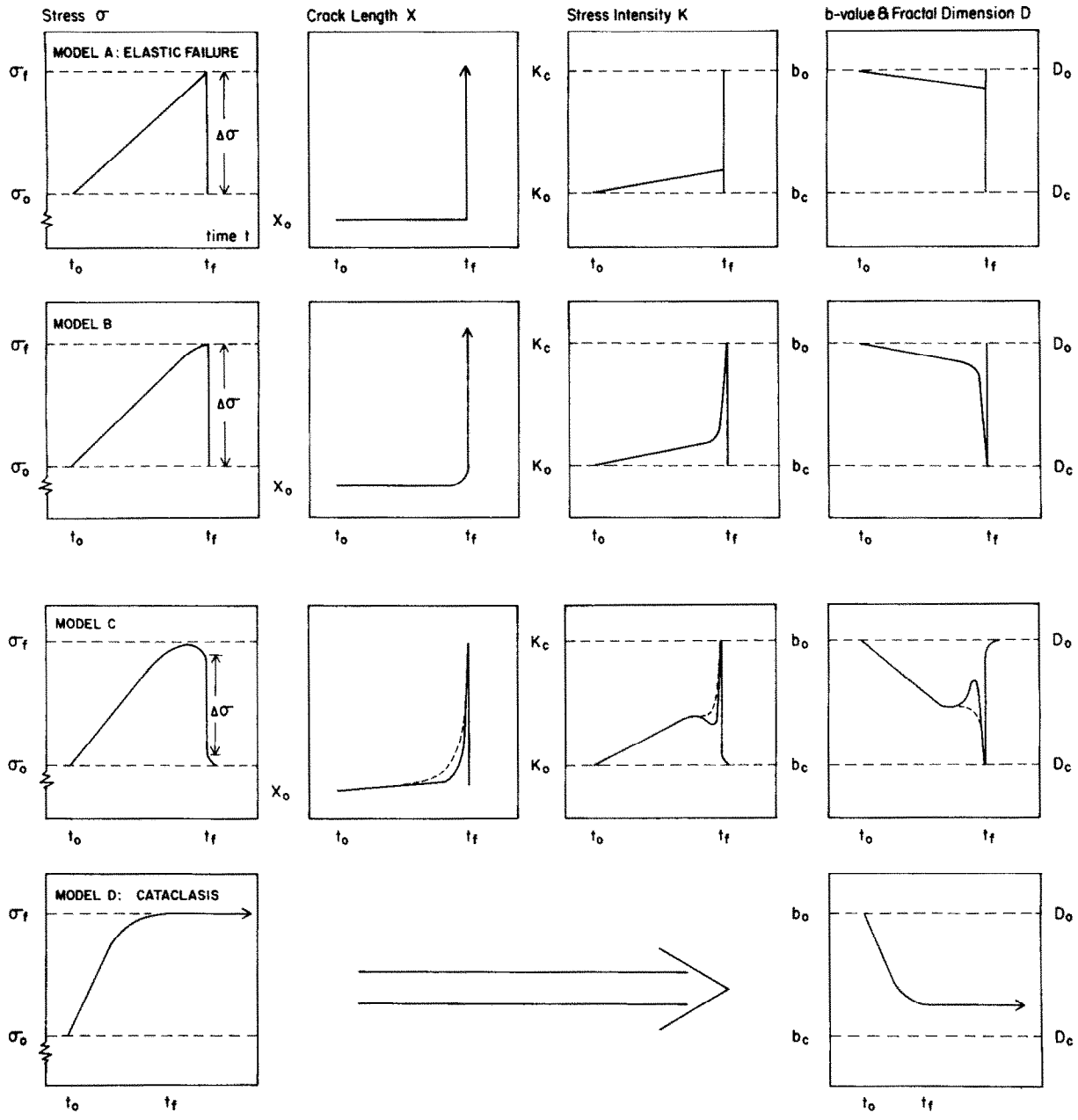

Fig. 2. Four variants of the proposed b-value anomaly model associated with different stress histories and levels of stress concentration. The stress, crack or fault length, stress intensity and b-value are plotted in columns, with the rows corresponding to the four model variants: A — elastic-brittle failure; B — strain hardening prior to dynamic rupture; C — strain softening prior to dynamic rupture; D — quasi-static deformation by cataclastic flow. All diagrams are normalised to the start time t_0 and the failure time t_f, and to the peak stress σ_f. X_0, σ_0, K_0 and b_0 are respectively initial values of the crack length, stress, stress intensity and b-value at time t_0. If t_0 is the time of occurrence of the previous event, then $b_0 \approx 1.2$. K_c and b_c are critical values of the stress intensity and b-value, and D is the power law exponent of the crack distribution. $D_c = 1$ and $D < 3$; therefore $b_c = 0.5$ and $b < 1.5$ for intermediate-size earthquakes, because $D = 2b$. Models A–D represent a gradation from purely elastic-brittle behaviour to macroscopically more ductile behaviour, with the dashed curve in model C corresponding to precursory stress drop dominated by slip behind an accelerating crack tip (which results in a decrease in stress but increase in stress intensity). These gradations can be modelled by gradations in the stress corrosion index, n, with higher values corresponding to more "brittle" behaviour. For model A, $n \to \infty$. For model D there is no stress concentration.

for four types of stress/strain behaviour. We assume a constant rate of strain at some remote boundary and plot all variables against time (Fig. 2). The first column of Fig. 2 shows the stress/time behaviour of the four models considered: A — elastic-brittle failure, B — dynamic failure after strain hardening, C — dynamic failure after strain softening, and D — quasi-static cataclastic flow. Cataclastic flow occurs at high confining pressures by pervasive fracture of the rock matrix rather than by shear localisation. Although this appears as "ductile" behaviour at the mesoscopic level, microscopically it is an entirely brittle mechanism. The four models listed above have been chosen from a continuum of cases and should not be thought of as definitive. Note that for model C the dynamic stress drop is less than the difference between the peak stress and the residual stress, because there is a quasi-static precursory stress drop and a small post-failure stress drop which occurs during the aftershock sequence. Models A and B have no quasi-static stress drop and, by definition, cataclastic flow involves no dynamic stress drop.

The second column shows the acceleration of the crack tip to critical velocities via eqn. (7). Model A requires instantaneous crack extension, where $n \to \infty$, and should be regarded as an ideal case rather than something that could be observed in nature. Model B would also require a high value of n to produce a sudden stress drop. Model C shows crack extension for two different values of n, the lower value (dashed line) corresponding to strain softening by precursory slip behind an accelerating crack front, and the higher value (continuous line) corresponding to the case where shear slip on subsidiary faults or pore fluid pressure changes are primarily responsible for the reduction in effective stress. No diagram is provided for the cataclastic flow case which, by definition, does not produce a dominant crack, and hence there is no macroscopic stress concentration. Model C is considered to be the physically most realistic case for real earthquakes, because a sudden stress drop as in models A and B would produce a discontinuous onset to the seismic pulse, and therefore infinite ground accelerations. However, because of the difficulties of sampling a continuous function, models A and B may serve as useful approximations in some cases.

The third column in Fig. 2 shows the combined effects of both stress and crack length on the stress intensity (again undefined for cataclastic flow because there is no macroscopic stress concentration) via eqn. (1). All models show that for most of the earthquake cycle the stress is the dominant term, but that accelerating crack extension dominates the crucial phase approaching critical rupture. For model C (continuous line) there may be a precursory minimum in stress intensity due to shear slip on subsidiary faults or pore fluid pressure changes, or an inflection (dashed line) if accelerating crack extension and slip behind the crack tip is dominant throughout the period of precursory stress decrease. (The latter process leads to a decrease in remote stress, but an increase in stress concentration due to dislocation pile-up at the crack tip (Stuart, 1979b).) The precursory minimum in stress intensity for model C may be related to seismic quiescence (e.g. Wyss, 1986), and Main and Meredith (1989) have suggested a possible classification of earthquake precursors based on this model. Model C predicts a long quiescent period (seismic gap) followed by intermediate-term precursors associated with the first peak in stress or stress intensity, then a period of relative quiescence correlated with a reduction in stress intensity, and finally short-term precursors immediately preceding dynamic rupture at near-critical stress intensities.

The fourth column shows the behaviour of the seismic b-value and the more fundamental crack distribution power law exponent D. All models show decreasing b-values over most of the seismic cycle, but only model C (continuous line) predicts the intermediate-term precursory b-value minimum often observed in nature (e.g. Jin and Aki, 1980; Carter and Berg, 1981; Imoto and Ishiguro, 1986). Model C is the only case which predicts an intermediate-term recovery after this minimum, or the increase in b-value reported by Smith (1981, 1986). This is indirect evidence of the crucial importance in the earthquake nucleation process of precursory seismicity off the dominant fault, and of fluid transport. Models A, B and C all predict dynamic failure at $b_c = 0.5$ (for $c = 1.5$ in

eqn. (12)), consistent with observed foreshock sequences. b_0 is the b-value at the onset of loading, which may be estimated for earthquake cycles to be up to about 1.2 (Von Seggern, 1980) by associating the onset of loading with termination of the aftershock sequence of the previous characteristic event. (In field examples we would expect at first a gradual transition from background seismicity levels ($b \approx 1$) to those associated with precursory seismicity around the dominant fault, so the "seismic gap" phase would be much less distinct than in the laboratory fracture of intact rock samples.) For model D, there is no dominant stress concentration and we have assumed that the b-value is negatively correlated with the level of stress, as first suggested by Scholz (1968a). Here, the b-value never reaches b_c because there is no critical fault rupture. Results presented in a later section, however, will demonstrate that the stress level alone is generaly insufficient to explain observed b-value anomalies.

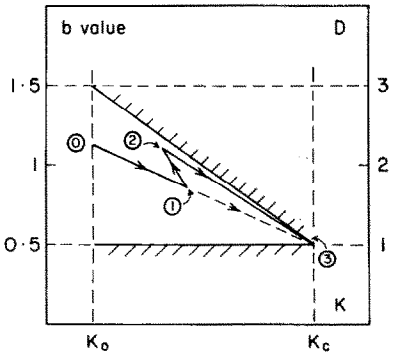

Fig. 3. Two different paths to critical rupture in $b-K$ space. Both of these paths (continuous and dashed lines) correspond to model C of Fig. 2. Changes in b-value can occur either by changes in fluid content (pore fluid pressure or partial pressure) or by changes in stress intensity. An increase in pore fluid pressure will reduce the event rate (Scholz, 1968b), but an increase in pore fluid activity will increase the event rate (Meredith and Atkinson, 1983), allowing the relative contributions to be compared. b_0 may take on any value between 0.5 and 1.5 for intermediate-size earthquakes, and here is taken to be about 1.2. Path 0–1–2–3 corresponds to precursory stress drop due to fluid diffusion, and path 0–1–3 corresponds to stress drop by precursory slip. Any straight line through the point ($K/K_c = 1$, $b_c = 0.5$) inside the boundaries delineated by the barbed lines corresponds to a constant pore fluid pressure. Because the value of b depends also on the period of the recording instrument, the crack length power law exponent, D (right-hand axis of figure), is the more fundamental parameter.

Finally, Fig. 3 illustrates the difference between the two variants of model C, both of which involve physically realistic strain softening prior to critical rupture. Paths are drawn in time through $b-K$ space to illustrate how a marked b-value recovery may be linked to changes in the activity of corrosive pore fluids as well as to changes in stress intensity. Scholz et al. (1973) considered only the mechanical effects of pore fluids, and suggested that quiescence would result from a decrease in stress following an influx of fluid into the dilatant volume. However, in laboratory experiments the mere presence of fluids at low pressure increases the rate of acoustic emissions (Meredith and Atkinson, 1983), so the net effect on event rates, like that on the b-values, will depend on the net effect of the fluids present.

To summarise, Fig. 2 illustrates examples of a generalised model that interprets temporal b-value variations in terms of the stress, chemical environment, crack length between asperities, and crack extension velocity. In the following sections we report to what extent the model predictions may be observed in the laboratory and in the field.

Laboratory data

Experimental details and data collection

Right cylindrical specimens of the test materials measuring 15 mm in diameter by 45 mm in length were deformed in compression at a nominally constant strain rate of $10^{-5}s^{-1}$ in a high-pressure triaxial apparatus (Edmond and Murrell, 1973). Compressed dry nitrogen gas was used to provide a hydrostatic confining pressure by means of a balanced piston arangement (Edmond and Murrell, 1973; Paterson, 1978), and a differential axial stress was applied via a 200 kN capacity ball-screw actuator. Specimens were deformed either air dried or water saturated.

A block diagram of the apparatus and its associated data measurement instrumentation is shown in Fig. 4. Stress and strain data were determined from load and displacement measurements monitored by external transducers, after correction for seal friction and elastic deformation of the loading piston. The loading pistons are hollow in order to

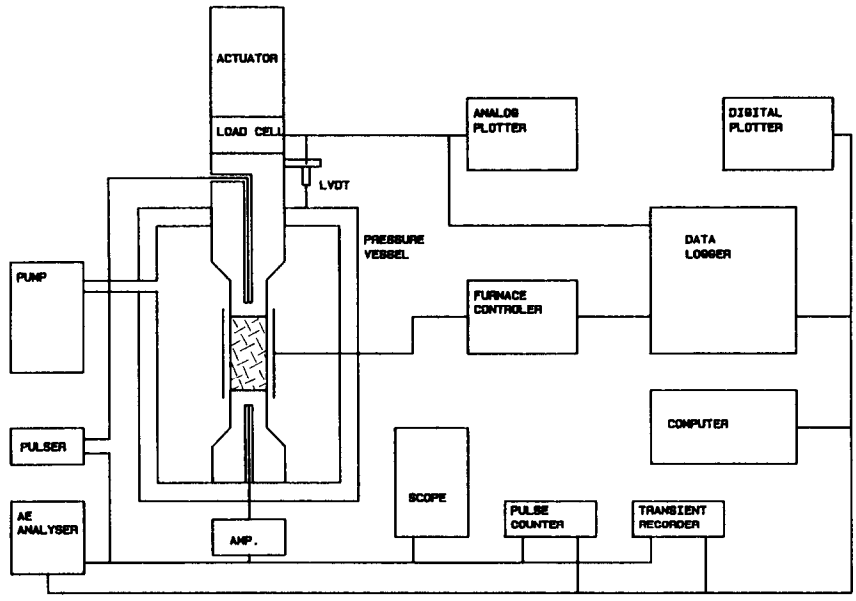

Fig. 4. Block diagram of the triaxial deformation apparatus used in this study, and its associated measurement and data acquisition instrumentation. Details are given in the text.

accommodate the ultransonic transducers used for measurement of acoustic wave velocity and acoustic emission (microseismicity) data.

For all of the experiments described in this paper, lithium niobate transducers with a resonant frequency of 1 MHz were used to monitor acoustic emission output, which was analysed using Dunegan/Endevco 3000 Series equipment. This equipment simultaneously records the rate of acoustic emission events, and the amplitude of each event. Acoustic signals were first amplified by a pre-amplifier with a fixed gain of 40 dB which is close-coupled to the deformation apparatus in order to provide a high signal to noise ratio. The pre-amplifier incorporates a high-pass filter which, together with the response curve of the transducer, limits the monitored frequency range to 700 kHz–1.5 MHz. Signals were then further amplified by a wide dynamic range logarithmic amplifier within the main body of the recording instrument. This logarithmic amplifier drives a threshold comparator and a peak voltage detector (range 0–100 dB, resolution 1 dB). Only when the amplifier output exceeds a pre-set threshold value does the threshold comparator turn on the peak voltage detector. The threshold level was set to exclude all signals received from the sample assembly set up within the pressure vessel at the desired confining pressure, but with no deviatoric stress applied (28 dB for the experiments described here). In this way, background noise was eliminated without affecting the peak amplitudes of real acoustic emission events. The output from the peak voltage detector was then compared with an internally generated, pulsed "staircase" voltage, and the number of pulses required to balance the voltages is equivalent to the amplitude of the event in decibels.

All discrete data were sampled at 20 s intervals, and rate data were also sampled over 20 s time intervals, throughout the duration of each test. The negative slopes of acoustic emission amplitude–frequency relationships (b-values) were determined for each time interval using the maximum likelihood method of Aki (1965), in which:

$$b = N \log e/(\Sigma M_i - NM_c) \text{ and } s = b/\sqrt{N} \quad (13)$$

where ΣM_i is the sum of all event amplitudes (c.f. earthquake magnitudes) having amplitudes exceeding M_c. M_c is defined as half the amplitude interval length (0.5 dB is this case) less than the lowest amplitude considered, N is the total number of events in the time interval considered, and s is the standard deviation of the calculated b-value.

Test materials

The Westerly granite used in this study was of the variety known as Westerly blue granite and samples were cored from the block of material described by Meredith and Atkinson (1985). The granite is even textured, having a mean grain size of 0.75 mm, and has a total porosity of approximately 1%.

The Darley Dale sandstone was from the same location as was the material described by Ismail and Murrell (1976), and is a well-indurated felspathic sandstone. The rock is poorly graded (grain sizes from 0.08 to 0.8 mm) with a total porosity of approximately 12%, and the cementing material is siliceous.

These materials were chosen for this study specifically because of their widely different mechanical properties which allowed us to simulate in the laboratory nearly all of the models of stress/time behaviour described earlier.

Experimental results

Results from a series of laboratory-scale rock fracture experiments designed to test as many variants of the proposed model as possible by contemporaneous monitoring of both deformation behaviour and acoustic emission (AE) signals are presented in Figs. 5–8. All data are plotted against time for ease of comparison with both field data and the model predictions. Note that when the assumption of constant strain rate is met, time and remotely applied strain are equivalent parameters.

Figure 5 shows data from a test on an air-dried sample of Westerly granite deformed under a confining pressure of 100 MPa. After a short non-linear period due to microcrack and pore closure, the stress/time curve (continuous line) is quasi-linear up to about 85% of the peak stress. This is followed by a dilatant, strain hardening phase leading to dynamic failure at peak stress. Such mechanical behaviour corresponds to our previously defined model B. The strain rate (broken line) remains essentially constant during elastic deformation, but increases significantly during the inelastic phase leading to failure.

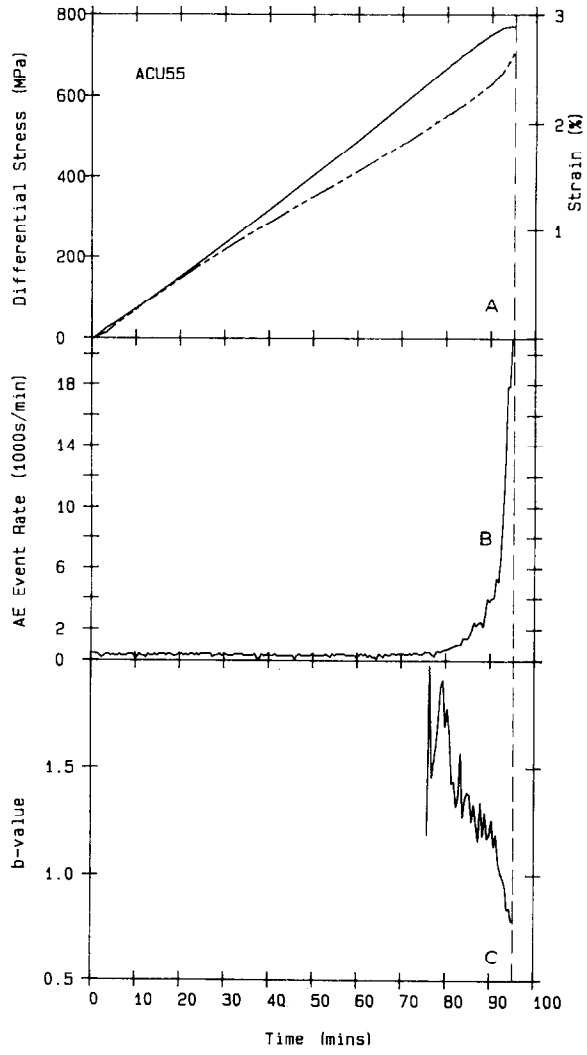

Fig. 5. Contemporaneous measurements of (A) differential stress (continuous line) and strain (broken line), (B) acoustic emission (AE) event rate and (C) *b*-value as functions of time for an air-dried sample of Westerly granite deformed at a nominally constant strain rate of 10^{-5} s^{-1} under a confining pressure of 100 MPa. The stress/time curve is quasi-linear over most of the loading cycle, and dynamic failure (dashed line) occurs at peak stress, after a short strain hardening phase. The strain/time curve is linear during elastic loading, but the strain rate increases during strain hardening. AE activity is essentially absent during the quasi-linear phase, but increases exponentially during strain hardening. *b*-values decrease monotonically during the strain hardening phase, and the curve is concave downwards as predicted for model B behaviour.

No significant level of AE activity above the threshold level was recorded during the linear elastic phase (Fig. 5B). However, when the stress/time curve deviates from linearity, indicat-

ing the growth of new microcracks, there is a corresponding rapid increase and acceleration in AE activity up to the point of failure. Figure 5C shows temporal variations in the *b*-value derived from the peak amplitudes of the events recorded in Fig. 5B. Because no emissions were recorded during linear elastic loading, it is not possible to determine *b*-values for most of the loading cycle. However, where a *b*-value can be calculated, it decreases monotonically with increasing stress, and is concave downwards as predicted by model B.

Figure 6 shows the same set of data as Fig. 5, but for a test on a water-saturated sample of Darley Dale sandstone deformed at 50 MPa confining pressure. The stress/time curve for this material (Fig. 6A, continuous line) is markedly non-linear, with peak stress followed by a significant precursory decrease in stress prior to dynamic failure on a well-defined fault plane and, finally, stable sliding along the fault (model C behaviour). In all experiments where failure occurred on a localised fault plane, this plane was oriented at an angle of between 30° and 35° to the axial differential stress. For data analysis purposes, we have defined dynamic failure as occurring when the negative slope of the stress/time curve is at a maximum ($\dot{\sigma}$ is at a minimum). Here the strain rate increases markedly during the inelastic strain hardening and strain softening phases due to the release of elastic strain energy from the loading system. The implications of this are discussed in a later section.

Again, the AE rate increases rapidly with the onset of dilatancy, which in this case occurs at little more than 50% of the peak stress. We can usefully separate dilatancy into two phases, the first dominated by the growth of new microcracks in the period up to peak stress, and the second dominated by the coalescence of existing microcracks to form a throughgoing fault in the period of post-peak strain softening. Around peak stress, the AE rate at first flattens out and then falls dramatically to a period of apparent quiescence. The dramatic quiescence associated with dynamic failure is caused by events becoming indistinguishable at critical crack coalescence. This masking effect produces a positive correlation between the *b*-value and the event rate in the phase

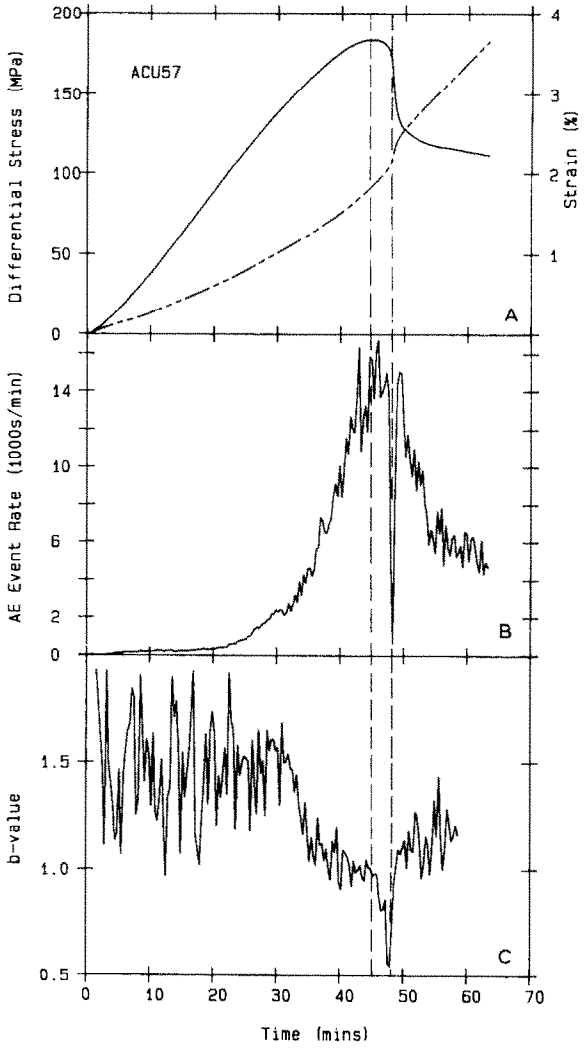

Fig. 6. Contemporaneous measurements of (A) differential stress (continuous line) and strain (broken line), (B) acoustic emission (AE) event rate and (C) *b*-value as functions of time for a water-saturated sample of Darley Dale sandstone deformed at a nominally constant strain rate of 10^{-5} s^{-1} under a confining pressure of 50 MPa. The stress/time curve is markedly non-linear, with a significant post-peak stress decrease prior to unstable faulting and stable sliding. The dashed vertical lines mark quasi-static and dynamic failure. Strain rate increases markedly during the inelastic phases, especially during strain softening. AE rate increases exponentially during the strain hardening phase leading to peak stress, but falls dramatically close to dynamic failure. Post-failure recovery and subsequent decay may be associated with aftershocks. A decreasing *b*-value associated with increasing stress leads to a broad minimum at peak stress followed by a short-term low *b*-value anomaly at failure. The critical *b*-value is close to the predicted value (model C) of 0.5. The *b*-value recovers in the post-failure phase.

associated with unstable failure, in contrast with the negative correlation observed throughout the quasi-static phases of the cycle. Hence, the masking effect of large events is thought to be significant in these experiments only in the dynamic phase. Immediately following instability the rate recovers, before finally decaying in a manner analogous to an aftershock sequence.

b-value data for this experiment are shown in Fig. 6C and exhibit all of the features predicted by model C (dashed line). During the early pseudo-elastic phase of loading, when there is a low level of AE activity, the *b*-value remains essentially constant, with a high value close to 1.5. At higher levels of stress, the major trend is one of a decreasing *b*-value, correlated with increasing AE rate and the growth of new microcracks, this rate flattening out at around peak stress. This is followed by an inflection point and a much shorter time-scale *b*-value anomaly which leads to dynamic failure close to the predicted value of 0.5 (for these triaxial compression experiments, $c = 1.5$ in eqn. (12) (Main et al., 1989), so that $b_c = 0.5$ and $D_c = 1$). Note that no precursory *b*-value recovery (model C, continuous line, Fig. 2) was observed in this experiment. A number of possible reasons for this are discussed in a later section. In the post-failure phase, the *b*-value recovers as expected. Thus the broad pattern of anomalies is entirely as expected if precursory slip behind an accelerating crack tip (which gives rise to a reduction is stress combined with an increase in stress intensity) is the dominant strain softening mechanism. This sigmoidal pattern prior to catastrophic rupture contrasts sharply with the concave-downwards, cusp-like anomaly expected and observed for model B behaviour. Note that the error in measurement of *b*-values is inversely proportional to $\sqrt{N}$, so that variability in *b*-values is much greater during the relatively quiescent low-stress phase of loading than during the dilatant phase when the AE rate is much increased.

Data from another of the tests on Darley Dale sandstone performed under experimental conditions identical to those from which the data of Fig. 6 were derived are presented in Fig. 7. This figure is included here as an indication of the repeatability of our experimental results for the important case where precursory strain energy release precedes dynamic failure. Note that all of the features described for the data of Fig. 6 can also be seen in Fig. 7. In particular, the precursory stress decrease, the phase of apparent seismic quiescence, and the second short-term *b*-value anomaly close to a value of 0.5 are all present.

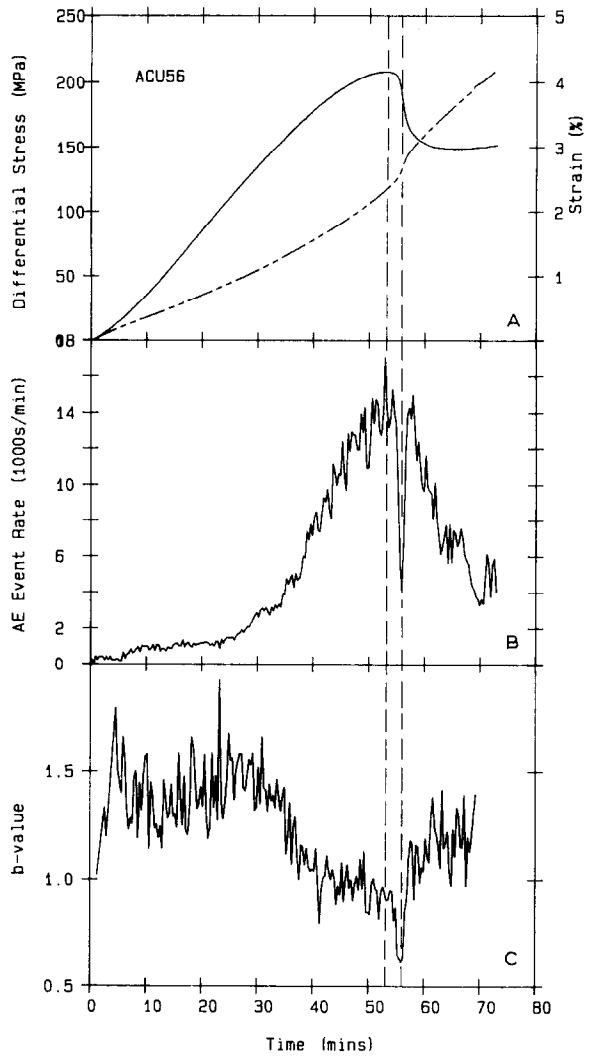

Fig. 7. The same suite of data as for Fig. 6, recorded for a sample of the same material deformed under the same experimental conditions. This figure is included to indicate the repeatability of our experimental results for the important case where strain softening precedes dynamic failure.

Finally, Fig. 8 shows data from a test on water-saturated Darley Dale sandstone conducted under a confining pressure (200 MPa) which is much higher than that used in the previously described experiments. In this case there is no

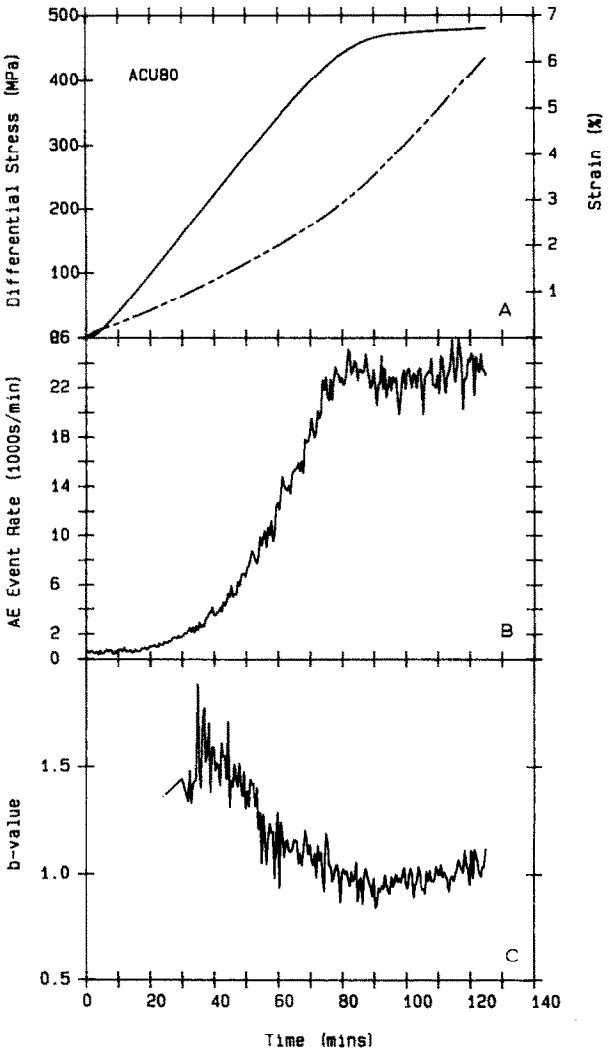

Fig. 8. Contemporaneous measurements of (A) differential stress (continuous line) and strain (broken line), (B) acoustic emission (AE) event rate and (C) *b*-value as functions of time for a water-saturated sample of Darley Dale sandstone deformed at a nominally constant strain rate of 10^{-5} s^{-1} under a confining pressure of 200 MPa. The stress/time curve shows no stress drop, and deformation occurs quasi-statically by cataclastic flow (model D). Strain rate increases by a factor of two between elastic loading and cataclastic flow phases. AE rate increases exponentially with the onset of microcracking, but remains at a consistently high level throughout the phase of cataclastic flow. The *b*-value is negatively correlated with the level of stress, but never approaches the critical value of 0.5 because there is no critical rupture.

stress drop, and deformation takes place quasi-statically by cataclastic flow (model D) rather than by dynamic rupture on a localised fault. In this case the strain rate increases by only a factor of two between the elastic loading and cataclastic flow phases. Under these conditions, the AE rate again increases with the onset of distributed microcracking, but remains at a consistently high level throughout the phase of cataclastic flow, with no indication of any period of quiescence. As expected for model D behaviour, the *b*-value is negatively correlated with the level of stress, and although it falls substantially from its initially high value of about 1.5, it never comes close to the critical value of 0.5 because there is no critical stress concentration leading to rupture.

Field data from the literature

Field data from a study (Imoto and Ishiguro, 1986) of temporal changes in seismicity rates and *b*-values preceding the Western Nagano, Japan, earthquake of 1984 ($M_s = 6.8$) are reproduced in Fig. 9. The seismicity rate data (upper diagram) exhibit two distinct periods of relatively low precursory activity, or quiescence, separated by a period of increased activity. Periods of enhanced activity and their related *b*-values are consistent with a broad classification of seismic precursors to failure, and are described in detail in Main and Meredith (1989). In particular, both a short-term and an intermediate-term minimum in the *b*-value are observed, and dynamic failure occurs very near the predicted critical value of 0.5. This pattern of behaviour is entirely as predicted by model C for the case of strain softening dominated by shear slip off the main fault and pore fluid diffusion, although the error bars show that the precursory *b*-value anomaly is at the limit of the resolution capability of the data. The critical *b*-value was found to be 0.58 ± 0.02.

In order to demonstrate that this is not an isolated observation, Fig. 10 (after Carter and Berg, 1981) also shows the predicted *b*-value anomaly for an event in the Tonga zone of the Tonga-Kermadec Trench in 1975 ($M_s = 7.8$), computed from the NOAA catalogue. Note the longer time scale of the anomaly associated with the larger earthquake.

The common features of the two data sets are as follows: (1) an increase in *b*-value, consistent with the transition from background seismicity

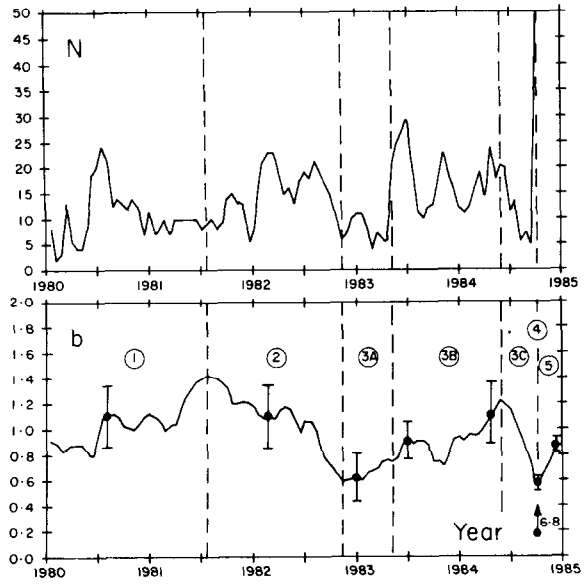

Fig. 9. Temporal variations in the seismic b-value for the Western Nagano earthquake of September 1984 (after Imoto and Ishiguro, 1986). All earthquakes with a completeness threshold $M_L > 1.5$, with focal depths shallower than 50 km, and with epicentres within 20 km of the epicentre of the mainshock (35.81° N, 137.55° E) were used to plot the diagram. The upper diagram shows seismic event rates in the foregoing 72 days plotted as a running average. The b-values were calculated using a Bayesian technique (Imoto and Ishiguro, 1986), to which we have added error bars of $\pm b/\sqrt{N}$ at selected points. The major precursory phases are 1 — transition from background b-value, 2 — strain hardening (decreasing b-value) and 3 — strain softening (increasing b-value followed by a short-term decrease near critical rupture). Phase 4 is the mainshock, and phase 5 the aftershock sequence. Phase 3 is split into two quiescent phases (3A and 3C) and a phase of enhanced activity (3B).

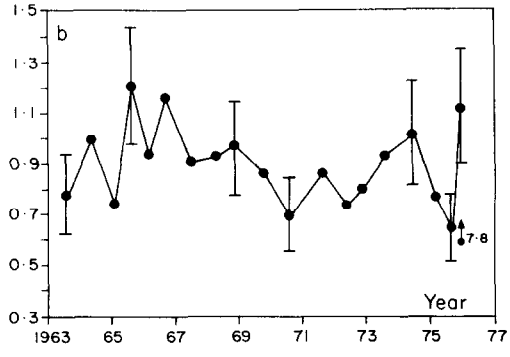

Fig. 10. Temporal variations in the seismic b-value for the December 1975 earthquake in the Tonga zone of the Tonga–Kermadec Trench (after Carter and Berg, 1981). All earthquakes with a completeness threshold $M_s > 4.5$ reported by the NEIS for the Tonga region were used to plot this diagram. The intermediate-term and short-term b-value anomalies are consistent with the predictions for model C.

($b \approx 1$) to the early stages of precursory seismicity associated with the main fault (phase 1 of Fig. 9), (2) a decrease in b-value consistent with strain hardening (phase 2), followed by a recovery, consistent with strain softening by a mechanism other than precursory slip on the main fault, and (3) a short-term decrease in b-value associated with such slip. The phase consistent with strain softening in Fig. 9 (phase 3) can be split into two quiescent phases (3A and 3C) and one active phase (3B). Because of the inferred increase in stress intensity, phase 3C is uniquely associated with accelerating slip. Phase 3B is considered most likely to be associated with the effect of fluids in enhancing seismicity rates, but this interpretation will require independent confirmation.

Finally, Smith (1986) reported several examples of a precursory intermediate-term increase in b-value followed by a short-term decrease with relative durations in the ratio 4 : 1. This is similar to the relative durations of the precursory increase and decrease in the b-value anomalies immediately prior to the mainshocks reported here (5 : 1 for Fig. 9; 3 : 1 for Fig. 10).

Discussion

Acoustic emissions and microcracking

It is an inherent assumption of this study that the acoustic emission (AE) activity monitored in our rock deformation experiments results from the growth and coalescence of microcracks, rather than from other AE-generating mechanisms such as twin formation or dislocation pile-up and motion. This seems to be a reasonable assumption if we consider the microstructural character of rocks (Kranz, 1983), the fact that all experiments were conducted at room temperature (Martin and Durham, 1975; Tullis and Yund, 1977; Carter and Kirby, 1978; Dunning et al., 1980), and the results of earlier laboratory studies (e.g. Mogi, 1968; Scholz, 1968a, b; Ohnaka and Mogi, 1982; Sano et al., 1982; Meredith and Atkinson, 1983; Fonseka et al., 1985) in which AE characteristics were directly related to cracking processes. In his comprehensive review, Kranz (1983) points out that while much theory exists on the role of microcrack

populations in rock fracture processes, there is a paucity of supporting observational data. Common assumptions include randomness in orientation and location of the initial microcrack population, and initial length–frequency distributions which can be Gaussian, exponential or power law in form. However, the assumption of randomness in the cracking process and stochastic independence between cracks becomes increasingly less acceptable as stress levels increase and cracks interact and coalesce as failure is approached (Kranz, 1983). We have incorporated these ideas into our theoretical modelling by electing to assume a power law distribution of microcrack lengths with a non-integer exponent which changes over time with a time-varying stress, reaching a critical value of unity at dynamic failure. Vere-Jones (1976, 1977) derived the probability of critical crack coalescence as stress increases and the length distribution changes, and concluded that the form of the length distribution function must be a power law to be compatible with the Gutenberg–Richter frequency–magnitude relationship for earthquakes.

The actual rate of AE activity depends on a number of factors, including rock type (Mogi, 1962; Boyce et al., 1981), testing machine stiffness (Kikuchi et al., 1981) and strain rate (Sano et al., 1982), in addition to the level of stress or stress intensity. Scholz (1968a) has reported that the start of AE activity corresponds to the onset of dilatancy (Brace et al., 1966). While the granite data reported here appear to support this idea, the sandstone data do not. Low but significant levels of AE activity are measured for Darley Dale sandstone even during the quasi-linear part of the stress/time curve (Figs. 6 and 7). Other workers (Kurita and Fujii, 1979; Gowd, 1980; Ohnaka and Mogi, 1982) have also observed AE activity prior to the onset of dilatancy in both sedimentary and igneous rocks. Such activity has been interpreted as due to friction between interlocking grains and the breaking of small asperities during compaction and crack closure under stress. However, once AE due to the growth of new microcracks commences, it is generally found to increase exponentially as the level of stress is increased (Scholz, 1968b; Gowd, 1980; Ohnaka and Mogi, 1982; Sondergeld et al., 1984). A preliminary exercise in curve fitting to the data of Figs. 6 and 7 has shown that the AE rate for these experiments also increases exponentially during the period of increasing stress, but that the decay in AE rate after dynamic failure is better described by a power law in a manner analogous to Omori's law for the decay of earthquake aftershocks (e.g. Utsu, 1972). This latter observation is consistent with our basic assumption of crack growth dominated by the mechanism of stress corrosion, because Das and Scholz (1981) were able to show that simple stress corrosion theory predicts Omori's law for aftershocks on a heterogeneous fault.

For all experiments where a period of strain softening (precursory stress decrease) preceded dynamic failure (e.g. see Figs. 6 and 7), the period of exponentially increasing AE was followed by a flattening off and then a rapid fall in AE rate to a period of apparent seismic quiescence. This phenomenon has been reported as occurring close to catastrophic failure in laboratory studies of rock fracture by a number of other workers (e.g. Gowd, 1980; Kikuchi et al., 1981; Sondergeld et al., 1984), but *only* when a strain softening phase preceded failure. For some earthquakes, a less dramatic but more extended quiescent phase has also been reported as preceding dynamic rupture (e.g. Imoto and Ishiguro, 1986; Wyss, 1986).

Quiescence may be a real or an instrumental phenomenon, and there are a number of possible explanations: (1) failure may be characterised by a small number of large-amplitude, long-duration events which could mask a large number of smaller events from the measuring instrument, resulting in an artificially low event rate, (2) failure may be marked by a very large number of small events running into one another, and appearing to the instrument as a single, small-amplitude, long-duration event, again resulting in a low event rate, or (3) there may only be events with amplitudes lower than the detection threshold. Ohnaka and Mogi (1982) and Sondergeld et al. (1984) report a frequency dependence of AE rate which they attribute to changes in microstructure during deformation. Once dilatancy is well developed, and microcracks interact and coalesce to form larger cracks, and hence larger source dimensions, the

lower frequency content of AE signals is found to increase. Under such conditions the higher frequency components would also be preferentially attenuated by the open, dilatant cracks. This observation is consistent with a general decrease in *b*-values during dilatancy, because larger cracks tend to generate AE events with larger amplitudes as well as lower frequencies. However, as catastrophic failure is approached a contrasting enhancement of high-frequency components was observed. Sondergeld et al. (1984) again interpreted this as being due to a change in source dimension. As crack coalescence relieves the applied stress by producing greater numbers of larger cracks during the phase of strain softening, eventually the relatively small barriers or ligamentary bridges (Swanson, 1987) between these larger cracks become the only remaining sites where crack extension can occur. New crack growth must, therefore, temporarily decrease in dimension, with a concomitant decrease in amplitude and increase in high-frequency content of the AE signals. This mechanism is consistent both with a recovery in *b*-value and with seismic quiescence explained by either of points (2) or (3) above. Both of these relative shifts in AE frequency can therefore be explained as manifestations of the microcracking process leading to macroscopic failure, although it is likely that explanation (2) applies to the laboratory results presented here, and (3) to field observations.

By contrast, where dynamic failure occurs at peak stress after a period of strain hardening (e.g. Fig. 5), the period of exponentially increasing AE is followed by a period of even more rapidly increasing AE rate in the final stage before rupture. Ohnaka and Mogi (1982) also observed this phenomenon for brittle failure of several igneous rocks in uniaxial compression and termed it a "supraexponential" increase. The observation that dynamic failure for the Westerly granite occurred at peak stress may be real, or may be a product of the data sampling rate with respect to the time scale of possible precursory phenomena.

Seismic b-values

In this discussion of *b*-value phenomena we concentrate on the behaviour described earlier for our model C, because this is the only model which predicts the precursory *b*-value recovery which has been observed to precede a number of major earthquakes (Jin and Aki, 1986; Carter and Berg, 1981; Smith, 1981, 1986; Imoto and Ishiguro, 1986), and we therefore consider it to be the physically most realistic model for the earth. Unlike models B and D, the *b*-value for model C cannot be simply correlated with the level of stress alone as has previously been suggested (Scholz, 1968a); it also depends on stress history (i.e. whether the level of stress is increasing or decreasing). More importantly, the *b*-value is quantitatively correlated with stress intensity (Fig. 1).

In our laboratory experiments we have been able to produce the two-stage *b*-value anomaly predicted by model C (Figs. 6 and 7), but with an inflection point rather than recovery to a precursory maximum in the period preceding dynamic rupture. There are a number of possible explanations for this. We have already discussed how an inflection point would be expected where precursory strain softening was dominated by crack coalescence and quasi-static fault slip without significant pore fluid diffusion. It should also be noted that our experiments were conducted at strain rates of approximately 10^{-5} s^{-1} — some nine orders of magnitude faster than inferred typical crustal rates. Under these conditions of relatively rapid loading, cracks may extend at a rate faster than that at which pore fluids are able to migrate into them. For example, for this very reason Atkinson and Meredith (1981) have suggested that stress corrosion crack growth in quartz is not influenced by environmental fluids above crack growth rates of about 10^{-3} ms^{-1}. This difference between crustal and laboratory strain rates is exacerbated by the fact that our assumption of a constant strain rate breaks down during the crucial phase of decreasing stress preceding dynamic failure, due to the rapid release of strain energy stored in the deformation apparatus. This problem is illustrated in Fig. 11 which shows stress, strain rate and stress rate data for the experiment for which AE data are given in Fig. 6. Dynamic failure is defined as occurring when the stress rate is at a minimum. Note how the strain rate increases rapidly during the period of decreas-

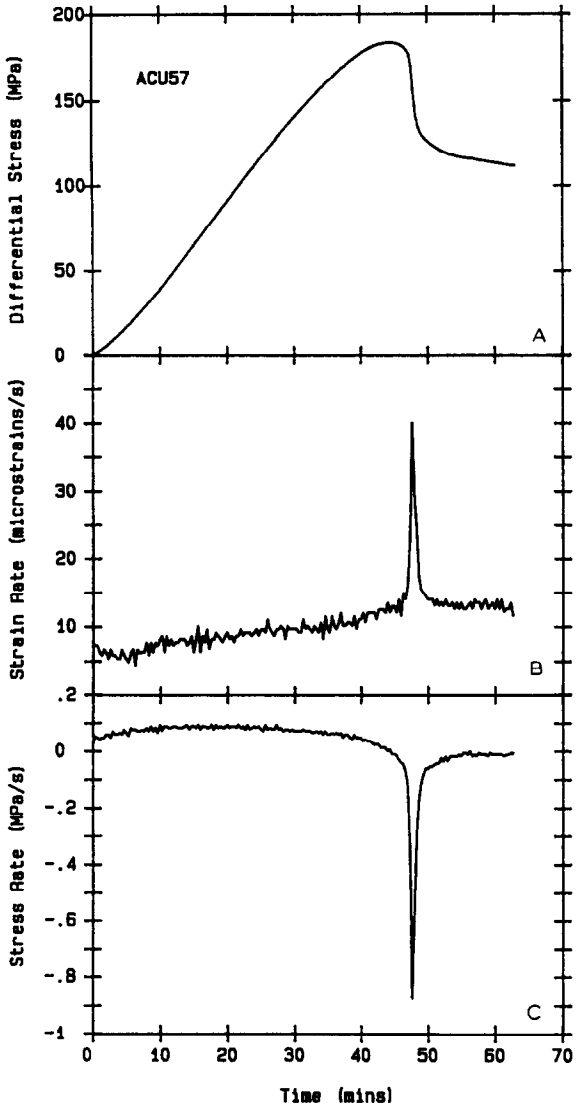

Fig. 11. Measurements of (A) stress, (B) strain rate, and (C) stress rate as functions of time for the experiment for which acoustic emission data are given in Fig. 6. The strain rate increases rapidly during the period of precursory stress decrease (negative stress rate), reaching a maximum at dynamic failure (defined as the minimum in stress rate).

ing stress (negative stress rate), reaching a maximum at dynamic failure. In future experimental work we will be able to alleviate this problem with the use of a new servo-hydraulic loading arrangement which will allow us to control the strain rate throughout the whole deformation cycle by means of servo-control of the loading system stiffness. The choice of a suitable loading system stiffness with respect to both *in-situ* stiffness and test sample stiffness in simulating quasi-static earthquake processes has been discussed by Walsh (1971), Goodman and Sundaram (1978) and Kikuchi et al. (1981).

The field observations of Imoto and Ishiguro (1986) for the Western Nagano earthquake (Fig. 9) also show the predicted two-stage *b*-value anomaly, but with a substantial recovery between the two minima. Qualitatively similar data are also reported by Carter and Berg (1981) for the magnitude 7.8 (M_s) event of 1975 in the Tonga zone of the Tonga–Kermadec Trench (Fig. 10). The field data of Figs. 9 and 10, although the most consistent with the predicted changes in seismicity available in the literature, exhibit considerable scatter about the predicted anomaly shape. This may be because they are subject to the transient effect of stress changes caused by nearby earthquakes, but is most likely to be because of statistical fluctuation. Moreover, in data recorded for the Western Nagano earthquake, but at an epicentral distance of 60 km rather than 20 km as in Fig. 9, the *b*-value anomaly pattern could barely be discerned above the background seismicity (Imoto and Ishiguro, 1986).

The field data are less statistically stable than the laboratory data because they were derived from the magnitudes of a smaller number of events. Indeed, for earthquakes with few foreshocks it may not always be possible to discern with sufficient statistical significance the second, short-term decrease in *b*-value.

Summary and conclusions

A comprehensive model based on the concepts of fracture mechanics and earlier laboratory experiments has been developed in this paper to explain the major temporal fluctuations in the seismic *b*-value over the complete cycle of loading, quasi-static failure and dynamic failure under a variety of conditions, in terms of the underlying physical processes of time-varying stress and stress corrosion crack growth at constant remote strain rate. The form of the *b*-value anomaly predicted by the model depends on the stress history. In particular, for the physically most realistic case where quasi-static failure is preceded by a period

of strain hardening, and dynamic failure is preceded by a period of strain softening, the model predicts two minima in the *b*-value separated by a temporary minimum or inflection point. These fluctuations in *b*-value are consistent with observed intermediate-term and short-term earthquake precursors separated by a period of seismic quiescence.

The experimental results reported here support the model predictions for a variety of imposed stress histories. In particular, both laboratory results for the case of precursory strain softening and field observations of several major earthquakes exhibit the short-term *b*-value anomaly, which is inconsistent with previous models based solely on the level of applied stress or the heterogeneity of the material. This implies that although it is also sensitive to changes in the partial pressure of water or water vapour, the *b*-value is a good indicator of the current level of stress intensity. Thus a unique interpretation of *b*-value changes in the crust requires, in principle, independent monitoring of fluid content (e.g. by electromagnetic measurements). Furthermore, the numerical value of the critical *b*-value for dynamic failure (0.5) is consistent with the predicted value of the crack length distribution exponent (D) for critical failure of unity, irrespective of humidity. This, in turn, is consistent with a geometric instability criterion based on critical coalescence of neighbouring fractures.

The final conclusion must be that although the work presented here is a significant advance in terms of earlier explanations of seismic *b*-values (where only stress level or material heterogeneity were considered), further laboratory experiments and field observations are required to validate fully the model. Future experimental work will concentrate on attempting to record an unequivocal two-stage *b*-value anomaly separated by a statistically significant recovery by maintaining a genuinely constant strain rate in slower strain rate tests with an independently controlled pore fluid pressure, and by testing geometrically more complex samples which better simulate fault asperities and barriers. More work is also necessary to establish under which field conditions (mainshock magnitude, magnitude threshold of complete reporting, depth of mainshock, annulus of locations around asperity) a statistically significant *b*-value anomaly over the whole earthquake nucleation cycle could be reliably obtained. Because the model proposed in this paper relates to asperity fracture, a dense network a few tens of kilometres from the epicentre of an event is probably a prerequisite for the reliable observation of the *b*-value anomaly suggested here for earthquake nucleation.

Acknowledgements

We thank Stan Murrell for generously providing unlimited access to the triaxial rock deformation system used in this study, and acknowledge his research grant (GR3/3691) from the British Natural Environment Research Council which enabled the construction of the acoustic monitoring system. We thank Masajiro Imoto and Makio Ishiguro for kindly providing the original data required for Fig. 9. Financial support for this work was provided in part by the British Natural Environment Research Council through research grants GR3/6293 and GR3/6812, and through a research studentship for Colin Jones (GT4/84/GS/130). Two anonymous reviewers are thanked for useful comments which have led to improvements in the paper.

References

Aki, K., 1965. Maximum likelihood estimate of b in the formula $\log N = a - bm$ and its confidence limits. Bull. Earthquake Res. Inst. Tokyo Univ., 43: 237–239.

Aki, K., 1981. A probabilistic synthesis of precursory phenomena. In: D.W. Simpson and P.G. Richards (Editors), Earthquake Prediction: An International Review. (Maurice Ewing Ser. 4). Am. Geophys. Union, Washington, pp. 566–574.

Anderson, O.L. and Grew, P.C., 1977. Stress corrosion theory of crack propagation with application to geophysics. Rev. Geophys. Space Phys., 15: 77–104.

Atkinson, B.K., 1980. Stress corrosion and the rate-dependent tensile failure of a fine-grained quartz rock. Tectonophysics, 65: 281–290.

Atkinson, B.K., 1982. Subcritical crack propagation in rocks: theory, experimental results and applications. J. Struct. Geol., 4: 41–56.

Atkinson, B.K., 1984. Subcritical crack growth in geological materials. J. Geophys. Res., 89: 4077–4114.

Atkinson, B.K. and Meredith, P.G., 1981. Stress corrosion cracking of quartz: a note on the influence of chemical environment. Tectonophysics, 77: T1–T11.

Atkinson, B.K. and Meredith, P.G., 1987a. The theory of subcritical crack growth with application to minerals and rocks. In: B.K. Atkinson (Editor), Fracture Mechanics of Rock. Academic Press, London, pp. 111–166.

Atkinson, B.K. and Meredith, P.G., 1987b. Experimental fracture mechanics data for rocks and minerals. In: B.K. Atkinson (Editor), Fracture Mechanics of Rock. Academic Press, London, pp. 477–525.

Atkinson, B.K. and Rawlings, R.D., 1981. Acoustic emission during stress corrosion cracking in rocks. In: D.W. Simpson and P.G. Richards (Editors), Earthquake Prediction: An International Review. (Maurice Ewing Ser. 4.) Am. Geophys. Union, Washington, pp. 605–616.

Båth, M., 1981. Earthquake magnitude — recent research and current trends. Earth Sci. Rev., 17: 315–398.

Boyce, G.M., McCabe, W.M. and Koerner, R.M., 1981. Acoustic emission signatures of various rock types in unconfined compression. In: V.P. Drnevich and R.E. Gray (Editors), Acoustic Emissions in Geotechnical Engineering Practice. Am. Soc. Test. Mater., Philadelphia, pp. 142–154 (ASTM STP 750).

Brace, W.F., Paulding, B.W. and Scholz, C.H., 1966. Dilatancy in the fracture of crystalline rock. J. Geophys. Res., 71: 3939–3953.

Caputo, M., 1976. Model and observed seismicity represented in a two-dimensional space. Ann. Geophys., 4: 277–288.

Carter, J.A. and Berg, E., 1981. Relative stress variations as determined by *b*-values from earthquakes in circum-Pacific subduction zones. Tectonophysics, 76: 257–271.

Carter, N.L. and Kirby, S.H., 1978. Transient creep and semibrittle behaviour of crystalline rocks. Pure Appl. Geophys., 116: 807–839.

Charles, R.J., 1958. Static fatigue of glass. J. Appl. Phys., 29: 1549–1560.

Charles, R.J. and Hillig, W.B., 1962. Kinetics of glass failure by stress corrosion. In: Symp. Resistance du Verre et les Moyens de l'Ameliorer. Union Sci. Cont. Verre, Charleroi, pp. 511–527.

Costin, L.S., 1987. Time-dependent deformation and failure. In: B.K. Atkinson (Editor), Fracture Mechanics of Rock. Academic Press, London, pp. 167–215.

Das, S. and Scholz, C.H., 1981. Theory of time-dependent rupture in the earth. J. Geophys. Res., 86: 6039–6051.

Demarèst, H.H., 1976. Application of stress corrosion to geothermal reservoirs. Los Alamos Sci. Lab., N. Mex., Rep. LA-6148-ms.

Dunning, J.D., Lewis, W.L. and Dunn, D.E., 1980. Chemomechanical weakening in the presence of surfactants. J. Geophys. Res., 85: 5344–5354.

Edmond, O. and Murrell, S.A.F., 1973. Experimental observations on rock fracture at pressures up to 7 kbar and the implications for earthquake faulting. Tectonophysics, 16: 71–87.

Fonseka, G.M., Murrell, S.A.F. and Barnes, P., 1985. Scanning electron microscope and acoustic emission studies of crack development in rocks. Int. J. Rock Mech. Min. Sci. Geomech. Abstr., 22: 273–289.

Goodman, R.E. and Sundaram, P.N., 1978. Fault and system stiffnesses and stick-slip phenomena. Pure Appl. Geophys., 116: 873–887.

Gowd, T.N., 1980. Factors affecting the acoustic emission response of triaxially compressed rock. Int. J. Rock Mech. Min. Sci. Geomech. Abstr., 17: 219–223.

Imoto, M. and Ishiguro, M., 1986. A Bayesian approach to the detection of changes in the magnitude–frequency relation of earthquakes. J. Phys. Earth, 34: 441–445.

Ismail, I.A.H. and Murrell, S.A.F., 1976. Dilatancy and the strength of rocks containing pore water under undrained conditions. Geophys. J. R. Astron. Soc., 44: 107–134.

Jin, A. and Aki, K., 1986. Temporal change in coda *Q* before the Tangshan earthquake of 1976 and the Haicheng earthquake of 1975. J. Geophys. Res., 91: 665–673.

Kanamori, H., 1978. Quantification of earthquakes. Nature, 271: 411–414.

Kanamori, H. and Anderson, D.L., 1975. Theoretical basis of some empirical relations in seismology. Bull. Seismol. Soc. Am., 65: 1073–1095.

Kikuchi, M., McNally, K. and Tittman, B.R., 1981. Machine stiffness appropriate for experimental simulation of earthquake processes. Geophys. Res. Letts., 8: 321–323.

King, G.C.P., 1983. The accommodation of large strains in the lithosphere of the earth and other solids by self-similar fault systems: the geometric origin of *b*-value. Pure Appl. Geophys., 121: 761–815.

Kranz, R.L., 1983. Microcracks in rocks: a review. Tectonophysics, 100: 449–480.

Kurita, K. and Fujii, N., 1979. Stress memory of crystalline rocks in acoustic emission. Geophys. Res. Letts., 6: 9–12.

Lama, R.D. and Vutukuri, V.S., 1978. Handbook of Mechanical Properties of Rocks. Trans Tech, Clausthal, Vol. II, 481pp.

Lankford, J., 1981. The role of tensile microfracture in the strain rate dependence of compressive strength of fine-grained limestone — analogy with strong ceramics. Int. J. Rock Mech. Min. Sci. Geomech. Abstr., 18: 173–175.

Lawn, B.R., 1975. An atomistic model of kinetic crack growth in brittle solids. J. Mater. Sci., 10: 469–480.

Lawn, B.R. and Wilshaw, T.R., 1975. Fracture of Brittle Solids. Cambridge Univ. Press, Cambridge, 204pp.

Li, V.C., 1987. Mechanics of shear rupture applied to earthquake zones. In: B.K. Atkinson (Editor), Fracture Mechanics of Rock. Academic Press, London, pp. 351–428.

Main, I.G., 1988. Prediction of failure times in the earth for a time-varying stress. Geophys. J., 92: 455–464.

Main, I.G. and Meredith, P.G., 1989. Classification of earthquake precursors from a fracture mechanics model. Tectonophysics, 167: 273–283.

Main, I.G., Meredith, P.G. and Jones, C., 1989. A reinterpretation of the precursory seismic *b*-value anomaly using fracture mechanics. Geophys. J., 96: 131–138.

Mandelbrot, B.B., 1982. The Fractal Geometry of Nature. Freeman, New York.

Martin, R.J. and Durham, W.B., 1975. Mechanisms of crack growth in quartz. J. Geophys. Res., 80: 4837–4844.

McCann, W.R., Nishenko, S.P., Sykes, L.R. and Krause, J., 1979. Seismic gaps and plate tectonics: seismic potential for major boundaries. Pure Appl. Geophys. 117: 1082–1147.

Meredith, P.G. and Atkinson, B.K., 1983. Stress corrosion and acoustic emission during tensile crack propagation in Whin Sill dolerite and other basic rocks. Geophys. J. R. Astron. Soc., 75: 1–21.

Meredith, P.G. and Atkinson, B.K., 1985. Fracture toughness and subcritical crack growth during high-temperature tensile deformation of Westerly granite and Black gabbro. Phys. Earth Planet. Inter., 39: 33–51.

Miachkin, V.I., Sobolev, G.A., Dolbilkina, N.H., Morozov, V.N. and Preobazensky, V.B., 1972. The study of variations in geophysical fields near focal zones of Kamchatka. Tectonophysics, 14: 287–293.

Mogi, K., 1962. Study of elastic shocks caused by the fracture of heterogeneous materials, and their relations to earthquake phenomena. Bull. Earthquake Res. Inst. Univ. Tokyo, 40: 125–173.

Mogi, K., 1967. Earthquakes and fractures. Tectonophysics, 5: 35–55.

Mogi, K., 1968. Source locations of elastic shocks in the fracturing process in rocks. Bull. Earthquake Res. Inst. Tokyo Univ., 46: 1103–1125.

Ohnaka, M. and Mogi, K., 1982. Frequency characteristics of acoustic emission in rocks under uniaxial compression and their relation to the fracturing process of failure. J. Geophys. Res., 87: 3873–3884.

Paterson, M.S., 1978. Experimental Rock Deformation — the Brittle Field. Springer, Berlin, 254pp.

Rikitake, K., 1976. Earthquake Prediction. (Developments in Solid Earth Geophysics, 9). Elsevier, Amsterdam.

Rikitake, K., 1987. Earthquake precursors in Japan: precursor time and detectability. Tectonophysics, 136: 265–282.

Rooke, D.P. and Cartwright, D.J., 1976. Compendium of Stress Intensity Factors. Procurement Executive, Ministr. Def., HMSO, London.

Sano, O. and Ogino, S., 1980. Acoustic emission during slow crack growth. Tech. Rep. Yamaguchi Univ., 2: 381–388.

Sano, O., Ito, I. and Terada, M., 1981. Influence of strain rate on dilatancy and strength of Oshima granite under uniaxial compression. J. Geophys. Res., 86: 9299–9311.

Sano, O., Terada, M. and Ehara, S., 1982. A study on the time-dependent microfracturing and strength of Oshima granite. Tectonophysics, 84: 343–362.

Scholz, C.H., 1968a. The frequency–magnitude relation of microfracturing in rock and its relation to earthquakes. Bull. Seismol. Soc. Am., 58: 399–415.

Scholz, C.H., 1968b. Microfracturing and the inelastic deformation of rock in compression. J. Geophys. Res., 73: 1417–1432.

Scholz, C.H., Sykes, L.R. and Aggarwal, Y.P., 1973. Earthquake prediction: a physical basis. Science, 181: 803–810.

Shimazaki, K. and Nakata, T., 1980. Time-predictable recurrence model for large earthquakes. Geophys. Res. Letts., 7: 279–282.

Sibson, R.H., 1982. Fault zone models, heat flow, and the depth distribution of earthquakes in the continental crust of the United States. Bull. Seismol. Soc. Am., 72: 151–163.

Sih, G.C., 1973. Handbook of Stress Intensity Factors for Researchers and Engineers. Inst. Fracture and Solid Mechanics, Lehigh Univ., Bethlehem, PA.

Smith, W.D., 1981. The *b*-value as an earthquake precursor. Nature, 289: 163–169.

Smith, W.D., 1986. Evidence for precursory changes in the frequency–magnitude *b*-value. Geophys. J. R. Astron. Soc., 86: 815–838.

Sondergeld, C.H., Granryd, L.A. and Estey, L.H., 1984. Acoustic emissions during compression testing of rock. In: Proc. Conf. Acoustic Emission/Microseismic Activity in Geologic Structures and Materials, 3rd. Trans Tech, Clausthal, pp. 131–145.

Stuart, W.D., 1979a. Quasi-static earthquake mechanics. Rev. Geophys. Space Phys., 17: 1115–1120.

Stuart, W.D., 1979b. Strain softening prior to two-dimensional strike-slip earthquakes. J. Geophys. Res., 84: 1063–1070.

Stuart, W.D., 1988. Forecast models for great earthquakes in the Nankai Trough subduction zone. Pure Appl. Geophys., 126: 619–641.

Swanson, P.L., 1987. Tensile fracture resistance mechanisms in brittle polycrystals: an ultrasonics and in-situ microscopy investigation. J. Geophys. Res., 92: 8015–8036.

Tullis, J. and Yund, R.A., 1977. Experimental deformation of dry Westerly granite. J. Geophys. Res., 82: 5705–5718.

Turcotte, D.L., 1989. Fractals in geology and geophysics. Pure Appl. Geophys., 131: 171–196.

Utsu, T., 1972. Aftershocks and earthquake statistics, IV. J. Fac. Sci. Hokkaido Univ., 3: 1–42.

Vere-Jones, D., 1976. A branching model for crack propagation. Pure Appl. Geophys., 114: 711–725.

Vere-Jones, D., 1977. Statistical theories of crack propagation. Math. Geol., 9: 455–481.

Von Seggern, D., 1980. A random stress model for seismicity statistics and earthquake prediction. Geophys. Res. Letts., 7: 637–640.

Walsh, J.B., 1971. Stiffness in faulting and in friction experiments. J. Geophys. Res., 76: 8597–8598.

Wiederhorn, S.M. and Bolz, L.H., 1970. Stress corrosion and static fatigue of glass. J. Am. Ceram. Soc., 53: 543–548.

Wyss, M., 1986. Seismic quiescence precursor to the 1983 Kaoki, Hawaii, earthquake. Bull. Seismol. Soc.Am., 76: 785–800.

Wyss, M., Habermann, R.E. and Griesser, J.-C., 1984. Seismic quiescence and aspertities in the Tonga–Kermadec arc. J. Geophys. Res., 89: 9293–9304.